Admittance Matrix Formulation of Waveguide Discontinuity Problems: Computer-Aided Design of Branch Guide Directional Couplers

FERDINANDO ALESSANDRI, GIANCARLO BARTOLUCCI, AND ROBERTO SORRENTINO, SENIOR MEMBER, IEEE

Abstract—A computational scheme is proposed which can be applied to the analysis of cascaded waveguide discontinuities of alternating boundary-enlargement and boundary-reduction type. Based on the mode-matching technique, the proposed procedure makes use of the admittance matrix characterization of waveguide stubs. With respect to the conventional *S*-matrix formulation, it leads to a notable reduction of the computational effort, particularly for lossless structures. At the same time, the criterion for avoiding relative convergence problems can be satisfied. The procedure has been used to set up a very accurate and efficient computer-aided design tool of branch guide couplers (BGC's) These are key elements of beam forming networks for multicontoured beam satellite antennas and have to be designed with very high accuracy so as to eliminate the necessity for tuning the components realized. Design accuracies better than 0.1 dB in *Ka*-band are demonstrated by experimental results.

I. Introduction

IN RECENT YEARS, special effort has been devoted to the development of high efficiency beam forming networks (BFN's) for multicontoured beam spacecraft antennas. Frequency reuse and multifunction antennas are replacing conventional spot beam antennas. As a result, the antenna system has notably grown in complexity, cost, and weight, and now has an important role in the definition of the payload architectures.

The BFN represents the heart of the antenna system. It has to generate the complex excitations necessary to shape the radiation pattern. Key requirements are wide band operation (up to 35 percent), high precision power division (typically 0.5 dB in amplitude and 5° in phase), high power capability (about 300 W CW), and reliable technology for space environment. To comply with the above requirements, the BFN makes use of branch guide directional couplers as elementary power dividers.

The BGC structure is schematically depicted in Fig. 1. Two rectangular waveguides are coupled by N branch guides connected along the broad walls. Additional degrees of freedom are obtained by allowing the main waveguide sections between the branches to have different heights, thus different impedances. These devices are machined with high precision milling tools and each component is made of two symmetrical halves corresponding to a cut in the middle of the broad waveguide wall. The two pieces are screwed together and they are not sensitive to contact imperfections because the cut is in the symmetry plane.

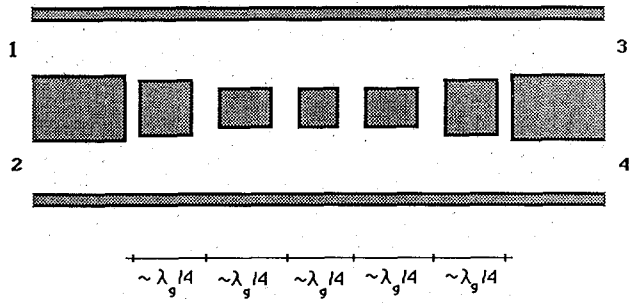

Fig. 1. Schematic of the branch guide coupler.

Several branch guide couplers are employed to generate the desired power division. They must be designed with extremely high accuracy in order to keep the total error at the output ports of the BFN below 0.5 dB.

Synthesis techniques of branch couplers by classical network theory have attained very high standards (see, for instance [1]–[5]), but are based on lumped or transmission line models that do not take into account parasitic effects at the waveguide junctions. Even with the inclusion of equivalent circuits of the discontinuities to compensate for these phenomena [6], [7], all higher order mode effects are not taken into account in an adequate way. As a result, each branch guide coupler must still be tuned with screws placed in appropriate locations in order to achieve the desired performance. Tuning screws not only require a time-consuming experimental activity, but also limit the maximum power transmittable and can generate passive intermodulation products.

These problems can be overcome by a very accurate design technique which would eliminate the necessity for tuning the components. Due to mathematical difficulties,

Manuscript received April 15, 1987; revised September 28, 1987. This work was supported in part by Selenia Spazio S.p.a. under Contract B3313010.

The authors are with the Department of Electronic Engineering, University of Rome "Tor Vergata," Rome, Italy.

IEEE Log Number 8718675.

0018-9480/88/0200-0394$01.00 ©1988 IEEE

it is not possible to include parasitics into a synthesis procedure. The high design accuracy required in the above-mentioned applications can only be obtained by numerical techniques. Though design techniques based on accurate field theoretical analyses have already been developed [8], one has also to bear in mind the computer efficiency of the analysis algorithm. This is of basic importance in keeping the overall CPU time within acceptable limits, since computer-aided design consists of a large number of repeated computer analyses according to some optimization strategy.

We have therefore first developed a field-theoretical analysis of the BGC structure using a mode-matching technique which accounts for most parasitics effects (except losses, which, in any case, must be kept at very low levels). At the same time, an efficient computational algorithm, based on an admittance-matrix formulation, has been set up.

The use of the admittance-matrix formulation for treating waveguide problems leads to several computational advantages. First, when losses are not to be considered, it allows the use of real instead of complex algebra. Second, the admittance matrix by definition lends itself to the characterization of two-port cavities with conducting walls. No matrix inversion is required, in fact, to evaluate the admittance matrix. This property can be used to obtain notable computational advantages when the structure is composed of alternating boundary-enlargement and boundary reduction discontinuities. Finally, the admittance matrix formulation is compatible with the criterion for avoiding errors due to the relative convergence phenomenon [10].

A computer-aided design tool of the branch guide coupler has been finally obtained by associating the computer analysis with an optimization routine. The experimental results have shown an excellent agreement with the theory. Computed values of the coupling show deviations less than 0.1 dB.

II. Computational Procedure

The BGC is usually modeled, in a first approximation, as two main transmission lines connected by N series branches. Such an oversimplified model leads to unacceptable discrepancies since it completely neglects any parasitic reactances due to the junction discontinuities. A more accurate model, as proposed in [5], includes T-junction equivalent circuits [9] to account for parasitic reactances. Also, this model has been proved to yield excessive disagreements with experimental results. It was found that higher order modes excited at the junctions not only contribute to reactive phenomena confined to the discontinuity region, but also produce a coupling between adjacent discontinuities. The T-junction equivalent circuit representation cannot be applied, as it is derived under the condition of an isolated junction.

To achieve the high accuracy required, it is necessary to develop a general analysis capable of accounting for all parasitic phenomena associated with higher order modes.

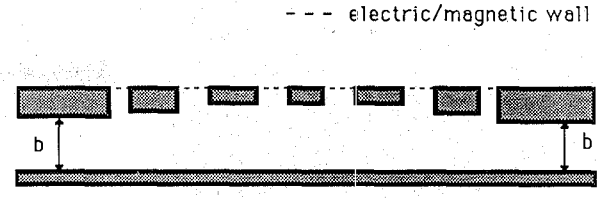

Fig. 2. Reduced structure for analysis.

As is usually done in the analysis of BGC's, the 4-port structure is first reduced to two 2-port structures by placing an electric or magnetic wall along the longitudinal plane of symmetry. The reduced half-structures, which correspond to odd- and even-mode excitations, respectively, consist of a main waveguide loaded with N short- or open-circuited stubs, as schematically indicated in Fig. 2. The following relations are used to compute the scattering parameters of the BGC from those of the reduced structures:

$$s_{11} = \left(s_{11}^{(e)} + s_{11}^{(o)}\right)/2 \qquad s_{12} = \left(s_{11}^{(e)} - s_{11}^{(o)}\right)/2$$
$$s_{13} = \left(s_{12}^{(e)} + s_{12}^{(o)}\right)/2 \qquad s_{14} = \left(s_{12}^{(e)} - s_{12}^{(o)}\right)/2$$

where s_{ij} are the BGC scattering parameters and $s_{ij}^{(e,o)}$ are those of the even (e) or odd (o) reduced structures. The remaining scattering parameters of the BGC are found from the above equations on the basis of reciprocity and symmetry considerations.

With simple modifications, all the results for the odd case can easily be extended to the even case. For brevity, from now on we will concentrate on the odd reduced structure. This structure can be regarded as the cascade of H-plane steps separated by uniform rectangular waveguides. Boundary-reduction steps alternate with boundary-enlargement steps. (In the even-mode case, waveguide sections with magnetic upper walls alternate with sections having electrical upper walls.)

The analysis of cascaded waveguide discontinuities is usually performed as follows. The generalized scattering matrices of the individual discontinuities are first computed by a mode-matching technique. The individual scattering matrices are then processed together with those of the uniform waveguide sections to get the overall characterization of the entire structure. Such an approach has been used extensively in the literature in a number of applications, from the design of E-plane metal insert filters [11] to the design of waveguide slot couplers [12], [13].

An alternative approach consists of using the transmission matrix representation. This approach has been shown to be computationally more efficient [14] but has some disadvantages. To be applicable, in fact, the T-matrix formulation requires the same number of field expansion terms to be retained at both sides of the discontinuity. This is in contrast with the criterion to avoid the relative convergence problem [10]. It is well known that to adequately represent the edge condition at the step so as to avoid incorrect numerical solutions, the mode number ratio must be as close as possible to the dimension ratio [15]. In addition, numerical instabilities may easily arise

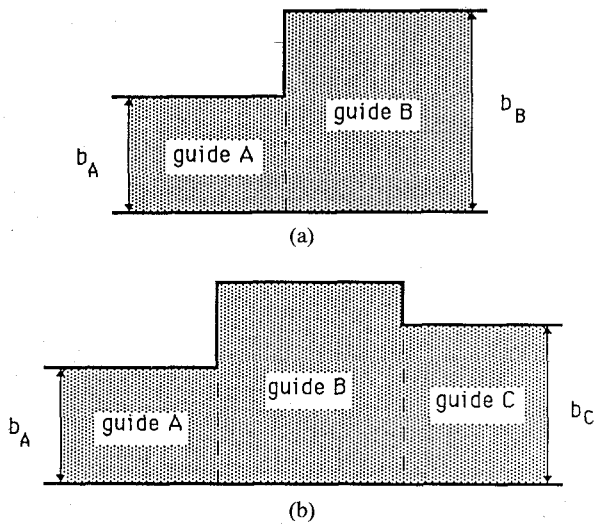

Fig. 3. (a) Enlargement-type step discontinuity. (b) Cascaded enlargement/reduction step discontinuities.

when a large number of higher order modes are retained or when the overall length of the uniform waveguide sections becomes too large [14]. To alleviate the problems associated with the T-matrix formulation, a modified formulation which combines the use of S- and T-matrix representations, has been recently proposed [16]. A different approach is proposed in this paper, which seems to be even less expensive, as discussed later on.

A. Modal Analysis of Step Discontinuity

With the notation of Fig. 3(a), according to the mode-matching technique, the transverse electric and magnetic fields are expanded in terms of normal modes at the two sides of the step discontinuity [9, p. 5][1]

$$\underline{E}_{tA} = \sum_n V_{nA}\underline{e}_{nA} \qquad \underline{H}_{tA} = \sum_n I_{nA}\underline{h}_{nA}$$
$$\underline{E}_{tB} = \sum_m V_{mB}\underline{e}_{mB} \qquad \underline{H}_{tB} = \sum_m I_{mB}\underline{h}_{mB} \tag{1}$$
$$n = 1,2,\cdots,N_A$$
$$m = 1,2,\cdots,N_B.$$

In (1) $\underline{e}_{nA}$ and $\underline{h}_{nA}$ are the transverse electric and magnetic field vectors of the nth (TE or TM) mode of waveguide A. Similarly, $\underline{e}_{mB}$ and $\underline{h}_{mB}$ are the transverse electric and magnetic field vectors of the mth mode of waveguide B. Explicit expressions for the above quantities are given in Appendix I. As customary, vector field quantities are orthonormalized over the waveguide cross section S, so that

$$\int_S \underline{e}_n \times \underline{h}_m \cdot \underline{dS} = \delta_{nm} \tag{2}$$

where δ_{nm} is the Kronecker delta. The numbers of expansion terms N_A and N_B in (1) have to be chosen in such a way as to avoid the relative convergence phenomenon; i.e. their ratio N_A/N_B must be as close as possible to b_A/b_B.

The boundary conditions for the E and H fields lead to a system of equations which can be put in the following form:

$$\boldsymbol{I}_A = [W]\boldsymbol{I}_B \tag{3a}$$
$$\boldsymbol{V}_B = [W]^T\boldsymbol{V}_A \tag{3b}$$

where $\boldsymbol{I}_A, \boldsymbol{V}_A$ and $\boldsymbol{I}_B, \boldsymbol{V}_B$ are arrays of dimensions N_A and N_B whose elements are the expansion coefficients of the transverse magnetic and electric fields ($\underline{h}_{nA}, \underline{e}_{nA}$, etc.) at the two sides of the discontinuity.

$[W]$ is a $(N_A \times N_B)$ matrix whose elements are given by

$$W_{nm} = \int_{SA} \underline{e}_{nA} \times \underline{h}_{mB} \cdot \underline{dS}. \tag{4}$$

Explicit expressions for W_{nm} are given in Appendix II. Index T stands for the transpose matrix.

Let us now observe that the boundary conditions at the discontinuity have led to the two sets of equations (3a) and (3b). This first set relates the currents at the narrow side A of the discontinuity to those at the wide side B. The other set relates the voltages at the wide side to those at the narrow side. In order to compute the scattering matrix or the transmission matrix representation of the discontinuty, the voltage and currents in (3) must be first decomposed into their incident and reflected components. It is then seen that one matrix inversion must be performed to compute either the scattering matrix S or the transmission matrix T. An admittance matrix Y of the step, on the contrary, cannot be defined.

B. Cascade of Two Discontinuities

In the case of two cascaded discontinuities, the conventional S-matrix computational scheme requires one matrix inversion for each discontinuity, plus one inversion to compute the overall S matrix. The last inversion is not necessary in the T-matrix approach, as it is replaced by matrix multiplication. In any case, at least *two matrix inversions* are required, one for each discontinuity.

We will show next that the computational effort can be notably reduced if the cascaded discontinuities are first of the boundary-enlargement type and second of the boundary-reduction type.

With reference to Fig. 3(b), the equations for the second step are

$$\boldsymbol{I}_C = [W']\boldsymbol{I}'_B \tag{5a}$$
$$\boldsymbol{V}'_B = [W']^T\boldsymbol{V}_C. \tag{5b}$$

$\boldsymbol{I}'_B$ and $\boldsymbol{V}'_B$ are the current and voltages of guide B at the second step discontinuity. They can be related to those at the first one using the telegraphists' equations for the normal modes of guide B. Using the admittance matrix representation, we may write

$$\boldsymbol{I}_B = \left[Y_{11}^{(B)}\right]\boldsymbol{V}_B + \left[Y_{12}^{(B)}\right]\boldsymbol{V}'_B$$
$$\boldsymbol{I}'_B = \left[Y_{21}^{(B)}\right]\boldsymbol{V}_B + \left[Y_{22}^{(B)}\right]\boldsymbol{V}'_B. \tag{6}$$

[1]To simplify the notation, no apparent distinction is made in (1) between TE and TM fields. Square brackets are used for matrices; boldface letters indicate arrays; and the underbar indicates vector quantities.

Because of the orthogonality of normal modes, the above matrices $[Y_{ij}^{(B)}]$ are diagonal matrices. Their expressions are quoted in Appendix III. Equations (3) and (5) can be combined through (6) to compute the overall Y-matrix representation of the cascade. One obtains

$$I_A = [W]\{[Y_{11}^{(B)}][W]^T V_A + [Y_{12}^{(B)}][W']^T V_C\}$$
$$I_C = [W']\{[Y_{21}^{(B)}][W]^T V_A + [Y_{22}^{(B)}][W']^T V_C\}. \quad (7)$$

The procedure described has led to the admittance matrix characterization of the cascaded discontinuities with *no matrix inversion*. Combining (3) and (5) to compute the scattering matrix or the transmission matrix representation of the cascaded discontinuities would require, on the contrary, one matrix inversion.

It is not surprising that the evaluation of the admittance matrix of Fig. 3(b) require a reduced computational effort compared with other matrix representations. The admittance matrix, in fact, appears by definition as the "natural" representation for cavities with ports realized on conducting walls. It could be easily seen that, when the first discontinuity is of the boundary-reduction type and the second one of the boundary-enlargement type, the impedance matrix can be computed with no matrix inversion, so it would be the most convenient representation. Grouping discontinuities in this way, however, would lead to matrices with larger dimensions since a higher number of modes has to be retained at the wide side of the discontinuities.

In conclusion, the above results demonstrate that the computational effort in the analysis of two cascaded discontinuities as in Fig. 3(b)—one boundary-enlargement and one boundary-reduction type—is substantially reduced by:

1) Considering the two cascaded discontinuities as a whole, i.e., as a 2-port structure. The matrix equations (3) and (5) at the ports are manipulated together to evaluate the overall matrix representation. One matrix inversion, instead of two, is required. Such an approach, based on the scattering matrix formulation, has been recently proposed in [18].

2) Adopting the admittance matrix representation. This permits the use of a real algebra and avoids any matrix inversion.

C. BGC Computational Procedure

We consider now the analysis of alternating boundary-enlargement and boundary-reduction discontinuities, as in Fig. 2. On the basis of the results of the previous section, to reduce the computational effort, boundary-enlargement and boundary-reduction discontinuities are grouped together so that the structure is considered as the cascade of N nonsymmetrical stubs separated by $N-1$ uniform waveguide sections (see Fig. 4). We suppose that M_i ($i = 1,2,\cdots,2N-1$) is the number of modes retained in the ith section. $M_0 = M_{2N}$ are the number of modes in the feeding waveguides.

With reference to Fig. 5, which shows the multiport network representation of two stubs connected by a waveguide section, the compuational procedure is as follows:

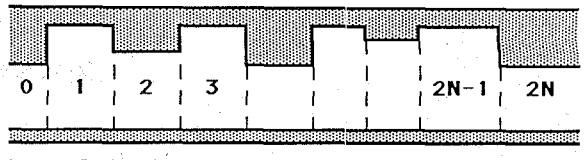

Fig. 4. Reduced structure of Fig. 2 as cascaded waveguide stubs.

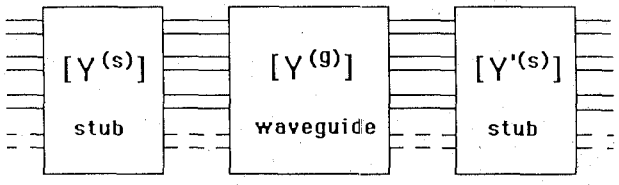

Fig. 5. Cascading admittance matrices.

TABLE I
CPU TIMES USING S-MATRIX OR Y-MATRIX FORMULATIONS FOR DIFFERENT NUMBERS OF MODAL EXPANSION TERMS IN THE FEEDING WAVEGUIDES

3 Branch-line coupler

Number of modes	4	5	6
S-matrix	0' 39".44	1' 13".75	2' 6".20
Y-matrix	0' 6".23	0' 10".14	0' 15".81
Time ratio	6.33	7.27	7.98

7 Branch-line coupler

Number of modes	4	5	6
S-matrix	1' 10".14	2' 21".21	4' 8".5
Y-matrix	0' 12".87	0' 24".26	0' 42".10
Time ratio	5.44	5.82	5.89

Quoted values correspond to the analysis of BGC's performed on a MicroVax II at 17 frequency samples.

1) Compute the Y matrix $[Y^{(s)}]$ of the first stub.
2) Compute the Y matrix $[Y^{(g)}]$ of the next waveguide section.
3) Compute the Y matrix $[Y'^{(s)}]$ of the next stub.
4) Compute the Y matrix $[Y]$ of the three cascaded networks according to the following equations:

$$[Y_{11}] = [Y_{11}^{(s)}] + [Y_{12}^{(s)}][Q] \cdot ([Y_{22}^{(g)}] + [Y_{11}'^{(s)}])[Y_{12}^{(g)}]^{-1}[Y_{21}^{(s)}]$$
$$[Y_{12}] = [Y_{21}]^T = -[Y_{12}^{(s)}][Q][Y_{12}'^{(s)}]$$
$$[Y_{22}] = [Y_{22}'^{(s)}] + [Y_{21}'^{(s)}][Y_{12}^{(g)}]^{-1} \cdot ([Y_{22}^{(s)}] + [Y_{11}^{(g)}])[Q][Y_{12}'^{(s)}] \quad (8)$$

with

$$[Q] = \{[Y_{12}^{(g)}] - ([Y_{22}^{(g)}] + [Y_{11}'^{(s)}]) \cdot [Y_{12}^{(g)}]^{-1}([Y_{22}^{(s)}] + [Y_{11}^{(g)}])\}^{-1} \quad (8')$$

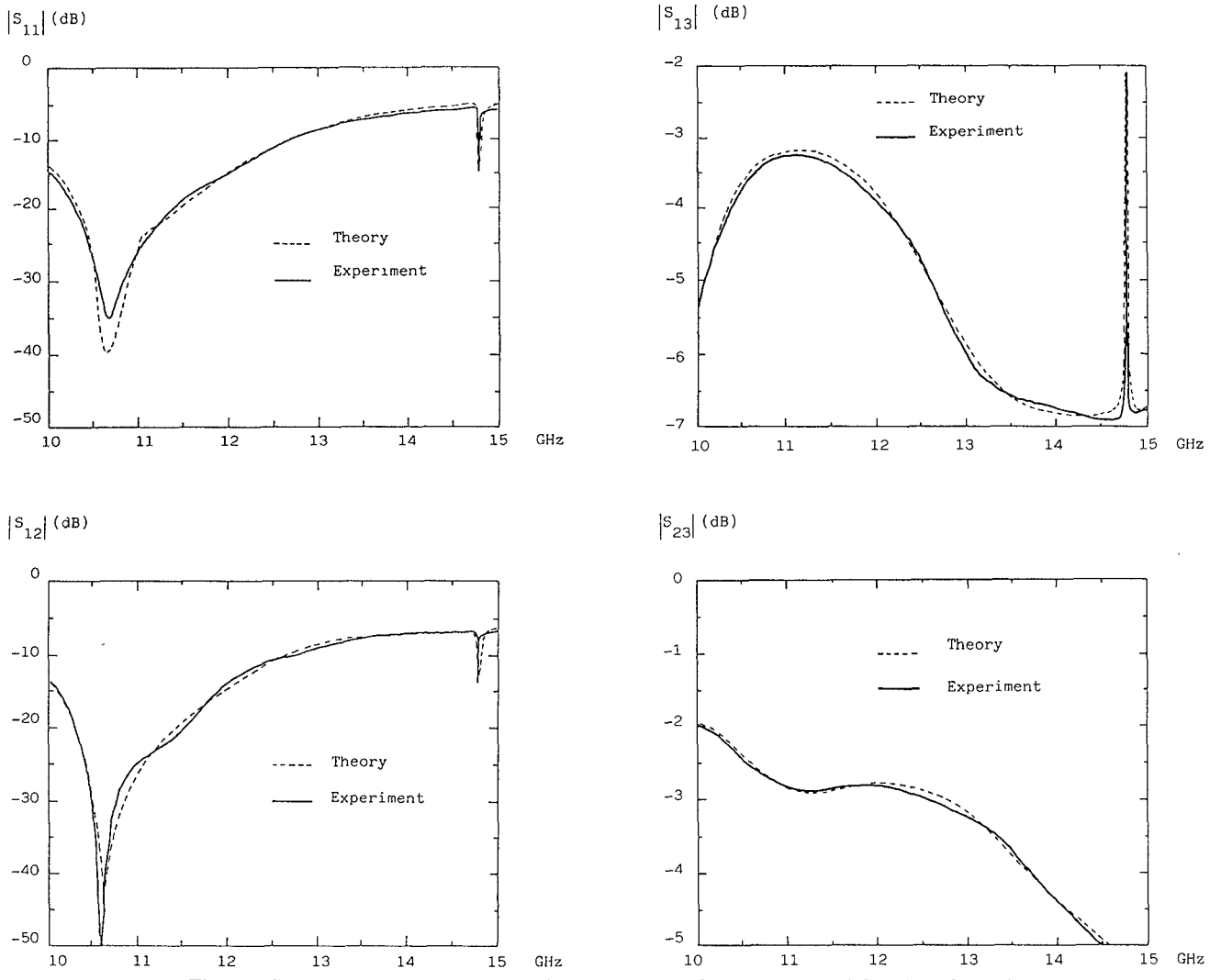

Fig. 6. Comparison between theory and measurements of an experimental three-branch coupler.

5) Go to step 2) unless the overall Y matrix is computed. After the first iteration, the Y matrix of the previous stub $[Y^{(s)}]$ on the right-hand sides of (6) is to be replaced by that of the structure computed in the previous iteration.
6) Compute the scattring parameters of the structure from the overall Y matrix resulting at the end of the above procedure.

Remembering that $[Y_{12}^{(g)}]$ is a diagonal matrix, the sequence of steps 2) through 5) requires only one matrix inversion to compute the Q matrix. This is done at step 4), i.e., when one stub is cascaded, through the waveguide interposed, to the remaining structure. The size of the matrix to be inverted is M_i $(i=2,4,6,\cdots,2N-2)$, i being the index of the waveguide section. The total number of inversions is equal to the number of waveguide sections; thus is $N-1$.

One additional inversion is required in step 6). The most straightforward (not the most efficient) procedure consists of computing the scattering matrix using the well-known matrix relation with the admittance matrix. This requires a matrix inversion of order $2M_0$. This procedure can substantially be simplified to get additional computational savings. For clarity of presentation, however, let us now compare the computational procedure illustrated so far with other, more conventional computational schemes. Further computational aspects will be discussed in the next section.

As stated above, the present procedure requires a number N of inversions[2] equal to the number of stubs and uses a real algebra.

The same technique of grouping boundary-reduction with boundary-enlargement discontinuities using the S matrix not only requires the use of complex numbers, but also N additional inversions to compute the S matrices of the stubs. Only the final inversion of step 6) is avoided, so that the total number of matrix inversions is $2N-1$, the sizes of the matrices to be inverted being M_i $(i=2,4,6,\cdots,2N-2)$ for the $N-1$ waveguide sections and $(M_{i-1}+M_{i+1})$ $(i=1,3,5,\cdots,2N-1)$ for the N stubs. The

[2] This figure, as well as those given below, refers to the structure of Fig. 4, i.e., to one half of the entire BGC structure. The symmetry of the BGC, which is usually present in practical structures, has not been taken into account. It would reduce the number of inversions by about one half.

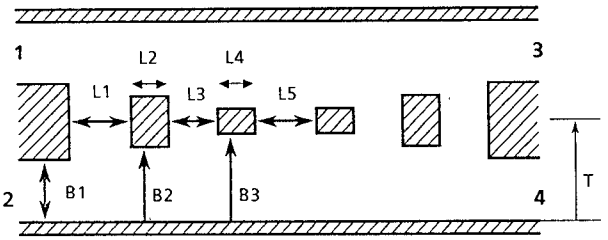

	COUPLER A N=3	COUPLER B N=5	COUPLER C N=5
B1	9.52	9 52	5 715
B2	9 40	9.52	5 715
B3		9.72	5.715
T	12 86	12.60	9.321
L1	4.79	1.70	0 747
L2	4.11	7 34	6 251
L3	8.68	3.40	1.938
L4		6.26	5.569
L5		4 53	2 501

Fig. 7. Dimensions (in mm) of the branch guide couplers of Figs. 6, 9, and 10, respectively. Connecting waveguide width $a = 19.05$ mm in all cases.

conventional S-matrix scheme, in which each discontinuity is analyzed separately, requires $3N$ matrix inversions.

Transmission matrix computational schemes require at least the same number of matrix inversions as the present approach. The latter, however, requires a much lower number of matrix multiplications. Taking into consideration its higher flexibility in the choice of the number of modes and the advantage of using a real algebra, the admittance matrix formulation presented here seems preferable over the transmission matrix approach.

We have finally developed two different computer programs using the Y-matrix and S-matrix formulations, both based on the concept of grouped discontinuities. A reduction of the computer time by a factor of about 6 is obtained with the Y-matrix formulation, as shown by the figures quoted in Table I.

An example of the excellent accuracy which is obtained is demonstrated in Fig. 6. The theoretical responses of an experimental three-branch coupler are compared with the measurements in the 10–15 GHz frequency band. The coupler's dimensions are given in Fig. 7 (coupler A). Only six to nine modes are taken into account in the various sections of the structure. The theory is fully capable of predicting also the very sharp peaks due to higher mode interaction between discontinuities.

III. Additional Numerical Considerations: Matrix Reduction and Numerical Instabilities

Step 6), the final step of the computational procedure described in the previous section, requires a matrix inversion of order $2M_0$ to compute the generalized scattering matrix from the generalized admittance matrix of the reduced BGC structure of Fig. 4. This is by far more than required. In all practical conditions, in fact, higher order modes on the terminating waveguide sections are evanescent and do not interact with the external circuit. Only the four scatering parameters associated with the fundamental modes are to be considered, while the rest of the S matrix is discarded.

Such a procedure, though straightforward, is clearly redundant and computationally inefficient. Actually, it is possible to carry out the entire computational procedure of the previous section with reduced matrix sizes in such a way that the resultant Y matrix of the structure is a 2×2 matrix involving only the dominant modes of the terminating waveguides.

Consider higher order modes excited at a discontinuity that are attenuated in such a way that they do not produce any interaction with other discontinuities. In a multiport equivalent network representation of the discontinuity, the ports corresponding to such modes are terminated by their characteristic impedances. These modes have been called localized modes in contrast with the accessible modes [17]. The number of ports connected to the external circuit is only that of the accessible modes, and the size of the matrix representation of the network can be reduced correspondingly.

After partitioning the complete admittance matrix according to the accessible (index a) and localized (index l) modes:

$$[Y] = \begin{bmatrix} [Y_{aa}] & [Y_{al}] \\ [Y_{la}] & [Y_{ll}] \end{bmatrix}$$

the reduced admittance matrix is given by

$$[Y^{\text{red}}] = [Y_{aa}] - [Y_{al}]([Y_{ll}] + \text{diag}[Y_c])^{-1}[Y_{la}] \quad (9)$$

where $\text{diag}[Y_c]$ is the diagonal matrix of the characterisitc admittances of the localized modes. Equation (9) involves a matrix inversion of size $M^{(l)}$ equal to the number of localized modes.

This matrix size reduction can be immediately applied at step 1) to the Y matrix of the first stub. All higher order modes on the left side (input waveguide) can be terminated by their characteristic admittance so that, using (9), the size of the Y matrix is reduced from $M_0 + M_2$ to only $1 + M_2$. We can proceed similarly with the last Nth stub, so that, at the end of the computational procedure, we end up with a 2×2 instead of an $M_0 \times M_0$ admittance matrix. The computation of the final step 6) can now be performed using direct formulas relative to 2-port networks.

The price to be paid involves the two inversions of order $M_0 - 1$ to evaluate the reduced Y matrices of the terminal stubs. This, however, is more convenient than performing one matrix inversion of order $2M_0$. One additional advantage is the size reduction of the matrices involved in the computational procedure.

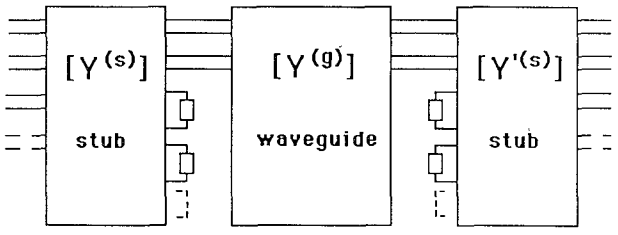

Fig. 8. Multiport equivalent network representation of cascaded stub–waveguide–stub with localized higher order modes.

The characterization in terms of reduced Y matrix can be advantageously applied also to the internal stubs. This technique not only implies some computational reduction, but also can avoid possible numerical instabilities. These are somewhat related to the concept of localized modes.

It has been pointed out that numerical instabilities may arise in the transmission matrix representation of cascaded waveguide discontinuities [14]. They occur when the overall length of the uniform waveguide sections is exceedingly large compared to the attenuation distance of the highest order mode.

In the admittance matrix formulation presented in this paper, numerical instabilities have been occasionally observed. They are due to the admittance matrix of a waveguide section interposed between two stubs. To be more specific, numerical overflows or underflows are associated with the product $\alpha_N l$, α_N being the attenuation constant of the highest order mode (which is below cutoff) and l the uniform waveguide length, i.e., the distance between the discontinuities.

When the product $\alpha_N l$ becomes excessively large, the corresponding term $\operatorname{cosech}(\alpha_N l)$ in $[Y_{12}^{(g)}]$ (see Appendix III) tends to zero and this matrix becomes singular. The procedure expressed by (8) leads to numerical instabilities.

These are easily avoided using the reduced admittance matrix of the stub. All the modes such that the product $\alpha_N l$ becomes too large are considered as localized modes and are eliminated from the admittance matrix of the waveguide. The computational procedure is still expressed by (8), with the exception that the Y matrices of the stubs are replaced by the corresponding reduced matrices. Fig. 8, which replaces Fig. 5, shows the multiport equivalent network representation of two stubs connected by a waveguide section. Localized modes appear as reactive loads of the stub networks and do not enter into the waveguide network representation.

For the sake of completeness, it is worth mentioning that the Y-matrix representation, as most network representations except the scattering matrix, possesses polar singularities.

The poles of the Y matrix of a stub are the resonant frequencies of the cavity obtained by short-circuiting the two apertures. Since they are known in advance, numerical problems can be avoided.

Additional singularities may arise in the computation of the reduced admittance matrix (9) when the matrix to be inverted becomes singular. This problem can be circumvented by cascading to the stub a short waveguide length before computing the reduced matrix. This has the effect of modifying the admittance matrix $[Y_{ll}]$ relative to the localized modes so eliminating the singularity of $[Y_{ll}]+\operatorname{diag}[Y_c]$.

According to our experience, singularity problems occur only in special cases. They may be encountered in some structures when analysis is performed with an extremely fine frequency step. The above-mentioned techniques to circumvent numerical instabilities affect only to a very small extent the computational effort.

IV. Design Procedure

The admittance matrix computational scheme described in the previous section has been associated with an optimization routine so as to obtain a complete CAD tool of the BGC.

The CAD procedure is as follows:

1) From the requirements of the BGC, a first approximate design is performed according to well-known procedures, such as, [3].
2) The response of the BGC is analyzed. Because of discontinuity effects, the response is generally shifted both in frequency and in amplitude.
3) To comply with the prescribed requirements an optimization routine is finally applied. This routine uses the gradient method to minimize the following error function:

$$F=\sum_{i=1}^{l}\left[\frac{\Delta C(i)}{\overline{\Delta C}}\right]^2+\sum_{i=1}^{l}\frac{|\bar{s}_{11}|^2}{|s_{11}(i)|^2}+\sum_{i=1}^{l}\frac{|\bar{s}_{12}|^2}{|s_{12}(i)|^2}$$

where summation is performed at l frequency samples. $\Delta C(i)$ is the difference between the nominal and computed coupling values; bars indicate desired tolerances. It was found that, in practical cases, $l=3$ sample points is sufficient to characterize the response in the entire band.

It is worth observing that the optimization procedure requires a large number of BGC structures to be analyzed at a limited number of fixed frequencies. As a consequence, the singularity problems mentioned in the previous section are never encountered in practice, while, on the other hand, it is very important to keep the computer analysis within reasonable time limits. The complete optimization procedure of a seven-branch coupler takes about 15 minutes of CPU on a MicroVax II.

Fig. 9 shows the theoretical and experimental results of a five-branch coupler designed to have a coupling $C=4\pm 0.15$ dB and an input reflection coefficient $|s_{11}|$ is better than 28 dB in the band 10.9–12.8 GHz. Dimensions of the coupler, designated as coupler B, are quoted in Fig. 7. A maximum discrepancy of 0.09 dB is found between theoretical and measured couplings. The BGC has been realized using a standard WR75 waveguide.

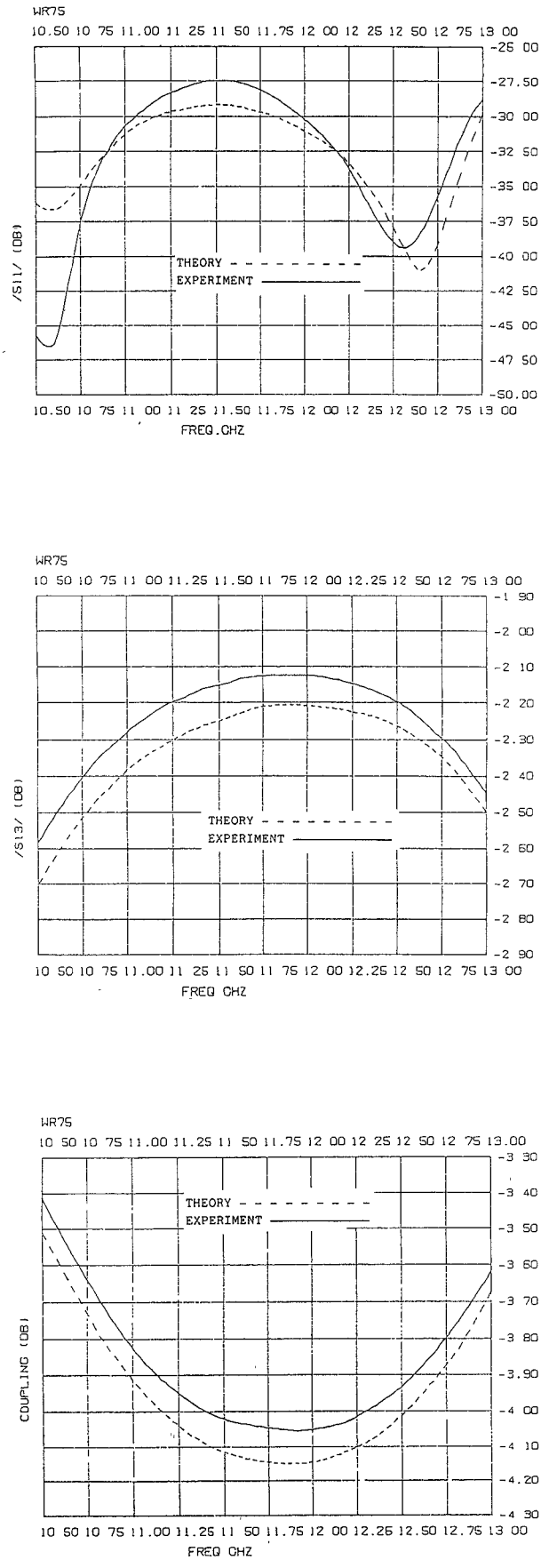

Fig. 9. Theoretical and experimental responses of an optimized five-branch coupler.

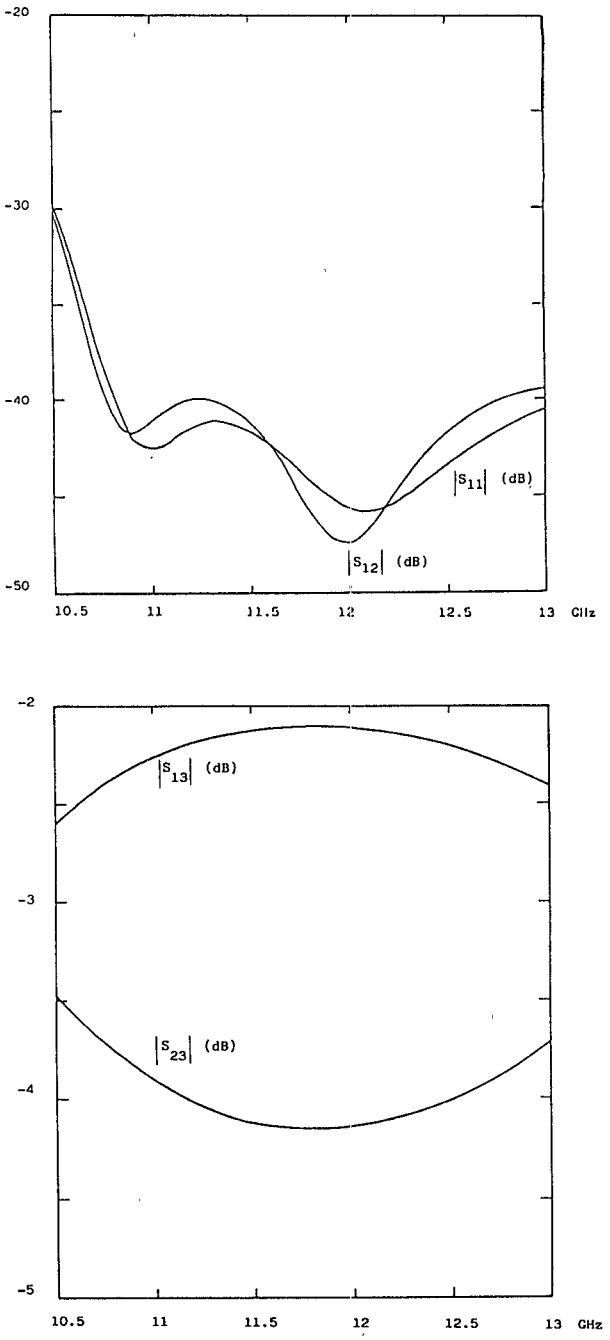

Fig. 10. Theoretical response of an optimized five-branch coupler in reduced-height waveguide.

A reduced-height waveguide was used to design the five-branch coupler (coupler C in Fig. 7) shown in Fig. 10. The WR 75 height was reduced by a factor of 0.6. This permits both a weight reduction and reduced coupling between discontinuities due to higher order modes. An input reflection coefficient better than 40 dB with a $\Delta C <$ 0.15 dB in the whole frequency band is demonstrated.

Appendix I

For the reader's convenience, the representation (1) of the EM field in terms of the normal modes in a rectangular waveguide section is detailed in this appendix.

The transverse components of the electric and magnetic fields are [9]

$$\underline{E}_t = \sum_n V_n \underline{e}_n = \sum_n V_n^{(h)} \underline{e}_n^{(h)} + \sum_n V_n^{(e)} \underline{e}_n^{(e)} \tag{A1}$$

$$\underline{H}_t = \sum_n V_n \underline{h}_n = \sum_n I_n^{(h)} \underline{h}_n^{(h)} + \sum_n I_n^{(e)} \underline{h}_n^{(e)}. \tag{A2}$$

The H-field eigenvectors $\underline{h}_n$ are related to the $\underline{e}_n$ by

$$\underline{h}_n = \underline{z}_0 \times \underline{e}_n.$$

The latter are obtained from the H-mode or E-mode potentials

$$\underline{e}_n^{(h)} = \underline{z}_0 \times \nabla_t \psi_n^{(h)} \qquad \underline{e}_n^{(e)} = -\nabla_t \psi_n^{(e)}. \tag{A3}$$

In the present case, because of the uniformity of the structure in the x direction, the x dependence of the EM field is determined by the incident field, which is assumed to be the dominant H_{10} mode. The potentials in (A3) therefore have the following expressions:

$$\psi_n^{(h)} = P_n^{(h)} \cos\frac{\pi x}{a} \cos\frac{(n-1)\pi y}{b}$$

$$\psi_n^{(e)} = P_n^{(e)} \sin\frac{\pi x}{a} \cos\frac{n\pi y}{b} \tag{A4}$$

where, in order for the orthonormalization condition (2) to be satisfied, the P coefficients are

$$P_n^{(h)} = \sqrt{\frac{2\delta_n}{ab}} \frac{1}{k_{n-1}} \qquad P_n^{(e)} = \frac{2}{\sqrt{ab}} \frac{1}{k_n} \tag{A5}$$

with

$$\delta_n = \begin{cases} 1 & \text{for } n = 1 \\ 2 & \text{for } n \neq 1 \end{cases} \tag{A6}$$

$$k_n = \sqrt{\left(\frac{\pi}{a}\right)^2 + \left(\frac{n\pi}{b}\right)^2} \tag{A7}$$

a and b being the waveguide dimensions.

Appendix II

The elements of the W matrix given by (4) represent the coupling between the modes in waveguides A and B occurring at the discontinuity between the two waveguides. The W matrix can be divided into the four submatrices $[W^{(hh)}]$, $[W^{(he)}]$, $[W^{(eh)}]$, and $[W^{(ee)}]$. We have, for instance,

$$W_{nm}^{(eh)} = \int_{S_A} \underline{e}_{n\mathrm{A}}^{(e)} \times \underline{h}_{m\mathrm{B}}^{(h)} \cdot \underline{dS} \tag{A8}$$

and similarly for the other submatrices.

Using the expressions given in Appendix I, one obtains

$$W_{nm}^{(h,h)} = P_{n\mathrm{A}}^{(h)} P_{m\mathrm{B}}^{(h)} k_{n-1,\mathrm{A}}^2 \cdot \frac{a}{2} b_{\mathrm{A}} \begin{cases} 1/\delta_n & \text{for } (n-1)R = m-1 \\ (-1)^n \dfrac{\operatorname{sinc}[(m-1)\pi/R]}{\left(\dfrac{n-1}{m-1}R\right)^2 - 1} \end{cases}$$

$$W_{nm}^{(h,e)} = P_{n\mathrm{A}}^{(h)} P_{m\mathrm{B}}^{(e)} (-1)^n \frac{\pi}{2} \sin(m\pi/R)$$

$$W_{nm}^{(e,h)} = 0$$

$$W_{nm}^{(e,e)} = P_{n\mathrm{A}}^{(e)} P_{m\mathrm{B}}^{(e)} k_{n\mathrm{B}}^2 \frac{a}{2} b_{\mathrm{A}} \begin{cases} 1/2 & \text{for } nR = m \\ \dfrac{nR}{m}(-1)^{n+1} \dfrac{\operatorname{sinc}(m\pi/R)}{\left(\dfrac{nR}{m}\right)^2 - 1} \end{cases}$$

$$m, n = 1, 2, 3, \cdots.$$

In the above expressions

$$\operatorname{sinc}(x) = \sin(x)/x$$

with a the common waveguide width and $R = b_{\mathrm{B}}/b_{\mathrm{A}}$ the ratio between the waveguide heights.

Appendix III

The generalized admittance matrix of a waveguide section of length l is given by

$$[Y] = \begin{bmatrix} [Y_{11}] & [Y_{12}] \\ [Y_{21}] & [Y_{22}] \end{bmatrix}$$

where the $[Y_{ij}]$ are diagonal matrices or order M, M being the number of modes retained in the waveguide section. Matrix elements have different expressions depending on whether an H or an E mode is considered.

For H modes

$$[Y_{11}] = \operatorname{diag}\left[\frac{-j\beta_n}{\omega\mu} \operatorname{cotan}(\beta_n l)\right] = \operatorname{diag}\left[\frac{-j\alpha_n}{\omega\mu} \operatorname{cotanh}(\alpha_n l)\right]$$

$$[Y_{12}] = \operatorname{diag}\left[\frac{j\beta_n}{\omega\mu} \operatorname{cosec}(\beta_n l)\right] = \operatorname{diag}\left[\frac{j\alpha_n}{\omega\mu} \operatorname{cosech}(\alpha_n l)\right]$$

$$[Y_{22}] = [Y_{11}] \qquad [Y_{21}] = [Y_{12}].$$

For E modes,

$$[Y_{11}] = \operatorname{diag}\left[\frac{-j\omega\epsilon}{\beta_n} \operatorname{cotan}(\beta_n l)\right] = \operatorname{diag}\left[\frac{j\omega\epsilon}{\alpha_n} \operatorname{cotanh}(\alpha_n l)\right]$$

$$[Y_{12}] = \operatorname{diag}\left[\frac{j\omega\epsilon}{\beta_n} \operatorname{cosec}(\beta_n l)\right] = \operatorname{diag}\left[\frac{-j\omega\epsilon}{\alpha_n} \operatorname{cosech}(\alpha_n l)\right]$$

$$[Y_{22}] = [Y_{11}] \qquad [Y_{21}] = [Y_{12}].$$

Trigonometric or hyperbolic functions are used depending on whether the mode is above or below cutoff, respectively. Correspondingly, β_n and α_n are the phase constant and attenuation constant.

ACKNOWLEDGMENT

Dr. F. Rispoli is gratefully acknowledged for his helpful contribution. The authors are also indebted to R. Flamini for useful discussions and for the excellent experimental work.

REFERENCES

[1] R. Levy, "Directional couplers," in *Advances of Microwaves*, vol. I, L. Young, Ed. London: Academic Press, 1966.
[2] L. Young, "Synchronous branch-guide directional couplers for low and high power applications," *IRE Trans. Microwave Theory Tech.*, vol. MTT-10, pp. 458–475, Nov. 1962.
[3] G. L. Matthaei, L. Young, and E. M. T. Jones, *Microwave Filters, Impedance Matching Networks, and Coupling Structures*. New York: McGraw-Hill, 1964.
[4] R. Levy and F. Lind, "Synthesis of symmetrical branch-guide directional couplers," *IEEE Trans. Microwave Theory Tech.*, vol. MTT-16, pp. 80–89, Feb. 1968.
[5] R. Levy, "Zolotarev branch-guide couplers," *IEEE Trans. Microwave Theory Tech.*, vol. MTT-21, pp. 95–99, Feb. 1973.
[6] R. Levy, "Analysis of practical branch guide directional couplers," *IEEE Trans. Microwave Theory Tech.*, vol. MTT-17, pp. 289–290, May 1969.
[7] E. Kuhn, "Improved design and resulting performance of multiple branch-waveguide directional couplers," *Arch. Elek. Übertragung.*, vol. 28, pp. 206–214, 1974.
[8] F. Arnt, D. Ellerman, H. W. Hausler, and J. Strube, "Field theory analysis and numerical synthesis of symmetrical multiple-branch waveguide couplers," *Frequenz*, vol. 36, pp. 262–266, Oct. 1982.
[9] N. Marcuvitz, *Waveguide Handbook*. New York: McGraw Hill, 1951.
[10] R. Mittra and S. Lee, *Analytical Techniques in the Theory of Guided Waves*. New York: Macmillan, 1971.
[11] Y. C. Shih, "Design of waveguide *E*-plane filters with all metal insert," *IEEE Trans. Microwave Theory Tech.*, vol. MTT-32, pp. 695–704, July 1984.
[12] F. Arndt *et al.*, "Field theory design of rectangular waveguide broad-wall metal-inset slot couplers for millimeter-wave applications," *IEEE Trans. Microwave Theory Tech.*, vol. MTT-33, pp. 95–104, Feb. 1985.
[13] H. Schmiedel and F. Arndt, "Field theory design of rectangular waveguide multiple-slot narrow-wall couplers," *IEEE Trans. Microwave Theory Tech.*, vol. MTT-34, pp. 791–797, July 1986.
[14] A. S. Omar and K. Schuenemann, "Transmission matrix representation of finline discontinuities," *IEEE Trans. Microwave Theory Tech.*, vol. MTT-33, pp. 765–770, Sept. 1985.
[15] Y. C. Shih and K. G. Gray, "Convergence of numerical solutions of step-type waveguide discontinuity problem by modal analysis," in *1983 IEEE MTT-S Int. Symp. Dig.* (Boston), pp. 233–235.
[16] R. R. Mansour and R. H. MacPhie, "An improved transmission matrix formulation of cascaded discontinuities and its application to *E*-plane circuits," *IEEE Trans. Microwave Theory Tech.*, vol. MTT-34, pp. 1490–1498, Dec. 1986.
[17] T. E. Rozzi and W. F. G. Meclenbrauker, "Wide-band network modeling of interactive inductive irises and steps," *IEEE Trans. Microwave Theory Tech.*, vol. MTT-23, pp. 235–245, Feb. 1975.
[18] G. Figlia, "Techniche veloci per l'analisi di una cascata di discontinuità in guida d'onda," in *Proc. VI National Conf. Appl. Electromagnetics* (Trieste), Oct. 1986, pp. 83–86.

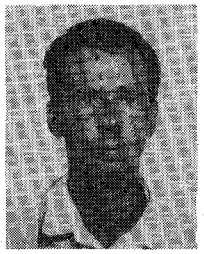

Ferdinando Alessandri was born in Rome, Italy, on June 26, 1959. He graduated cum laude in electronic engineering from the University of Roma "La Sapienza" in 1986 with a thesis on the design of branch guide directional couplers for satellite communications. His current research activities are in the field of microwave circuits.

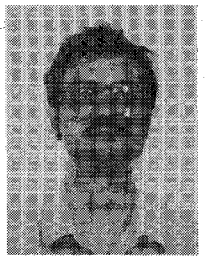

Giancarlo Bartolucci was born on September 22, 1958, in Rome, Italy. He graduated cum laude from the University of Rome "La Sapienza" in 1982 with a thesis on integrated optics.

In 1982 he was with Fondazione U. Bordoni, Rome, Italy. In 1983 he served as Officer in the Technical Corps of the Army. Since 1984 he has been with the Department of Electronic Engineering at the University of Rome "Tor Vergata" as a research assistant. His current research interests are in the field of microwave and millimeter-wave transmission lines.

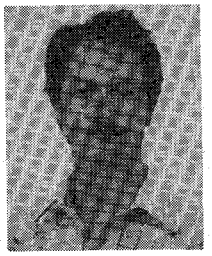

Roberto Sorrentino (M'77–SM'84) received the "Laurea" degree in electronic engineering from the University of Rome "La Sapienza," Rome, Italy, in 1971.

In 1971 he joined the Department of Electornics at the same university, where he was an Assistant Professor of Microwaves. He also was an Associate Professor at the University of Catania (1974–76) and at the University of Ancona (1976–77). From 1977 to 1985 he was with the University of Rome "La Sapienza" as an Associate Professor of Solid State Electronics (1977–1982) and Microwave Measurements (1982–1985). In 1983 and 1986 he was appointed a Research Fellow at the University of Texas at Austin, Austin, TX. Since 1986 he has been a full Professor of Microwaves at the University of Rome "Tor Vergata." His research activities have been concerned with electromagnetic wave propagation in anisotropic media, numerical methods for microwave and millimeter-wave structures, and the analysis and design of microwave and millimeter-wave integrated circuits.